ELSEVIER

Thermochimica Acta 400 (2003) 61–67

thermochimica acta

www.elsevier.com/locate/tca

The mechanism of reduction of iron oxide by hydrogen

Hsin-Yu Lin [a], Yu-Wen Chen [a,*], Chiuping Li [b]

[a] *Department of Chemical Engineering, National Central University, Chung-Li 32054, Taiwan*
[b] *Division of Fine Chemicals and Solvents, Chinese Petroleum Cooperation, Chia-Yi 60036, Taiwan*

Received 21 June 2002; received in revised form 9 September 2002; accepted 10 September 2002

Abstract

Precipitated iron oxide samples were characterized using temperature-programmed reduction. H_2 was used as the reduction agents. The two-stage reduction was observed: Fe_2O_3 was reduced to Fe_3O_4 and then reduced to metallic Fe. The activation energy for the two reduction steps of iron oxide are 89.13 and 70.412 (kJ mol^{-1}), respectively. The simulation by reduction models of the TPR patterns presents well fitting of unimolecular model for $Fe_2O_3 \rightarrow Fe_3O_4$ reduction and two-dimensional nucleation according to Avarmi–Erofeev model for $Fe_3O_4 \rightarrow Fe$.

Keywords: Temperature-programmed reduction; Iron oxide; Kinetic mechanism

1. Introduction

Temperature-programmed reduction (TPR) method has been widely used in the characterizations of solid materials [1–10]. Kissinger [11] developed a method to demonstrate the effect of varying order of reaction from differential thermal analysis (DTA) patterns. Wimmers et al. [5] presented a convenient method extended from Kissinger's approach for the calculation of TPR patterns by using kinetic expressions.

Many works have been done on the reducibility of bulk iron oxides by TPR. Brown et al. [8] studied the reducibility of bulk iron oxide materials and showed that the reducibility of Fe_2O_3, as measured by TPR, differed markedly from that of Fe_3O_4. The first step in the reduction of Fe_2O_3 is reduction to Fe_3O_4, which was confirmed by the TPR profiles, with the low-temperature peak in the profile of Fe_3O_4 reduction corresponding to this reaction.

Unmuth et al. [12] studied the reduction using TPR technique. They prepared the catalysts by loading metal on silica gel, and calcined in air at 200 °C. They found that the reduction profile for 5 wt.% Fe/SiO_2 consisted of two peaks, at 307 and 447 °C, which correspond to the following process:

$$Fe_2O_3 \rightarrow Fe_3O_4 \rightarrow Fe$$

TPR data for α-Fe_2O_3 and Au/α-Fe_2O_3 systems was reported by Munteanu et al. [13], they also found that the TPR profiled for α-Fe_2O_3 consisted of two peaks, at 280 and 427 °C. It must be emphasized that the literature data diverge to a large extent [6–13], since different oxides exist (Fe_2O_3, Fe_3O_4 and FeO) and, moreover, these can contain impurities or dopants. Furthermore, there are large differences in the literature with respect to, for instance, the selection of reduction temperature, the particle/crystallite size, and the reducing agent. The present study gives TPR results of different heating rate, and shows the good agreement of the TPR simulation results compared

* Corresponding author. Fax: +886-3-425-2296.
E-mail address: ywchen@cc.ncu.edu.tw (Y.-W. Chen).

0040-6031/03/$ – see front matter
PII: S0040-6031(02)00478-1

with experiment data. The objective of this investigation was to gain a more systematic understanding of the reducibility of iron oxide.

2. Experimental

2.1. Materials

Precipitated sample was prepared using $Fe(NO_3)_2 \cdot 9H_2O$ from Fisher Chemical Co. The iron oxide was prepared by a precipitation method. An aqueous solution containing $Fe(NO_3)_3$ and a second solution containing aqueous NH_3 (~2.7 M) were maintained in stirred glass vessels at 83 °C. The two solutions were separately conveyed by fluid pumps to a stirred tubular reaction vessel that was maintained at 82 ± 1 °C. Precipitation (to form FeOOH/ Fe_2O_3) occurred as the two solutions were pumped upward through the vessel, while an in-line pH electrode was used to monitor the pH of the reactor effluent. The flow rate of NH_3 solution was normally fixed at 60 ml/min, while that of the Fe^{3+} solution was adjusted (typically to 90 ml/min) to give a precipitation pH value of 6.0 ± 0.2. Collection of the precipitate was made in ice-cooled vessels and was continued until one of the two solutions was consumed. The precipitate was then thoroughly washed by vacuum filtration to remove excess NH_3 and NO_3^-, using 10 l of deionized, distilled water per 100 g (dry weight) of final catalyst. The washed precipitate was dried in a vacuum oven for 60 h at 50 °C, to remove most of the excess water, and then for an additional 24 h at 120 °C. The product was dried further in a vacuum oven for 16 h at 120 °C.

2.2. Temperature-programmed reduction

Temperature-programmed reduction studies were performed using 5% H_2/N_2. The consumption of H_2 was measured by the change in thermal conductivity of the effluent gas stream, and a dry ice/acetone bath was used to remove water formed during the hydrogen reduction. Catalyst sample weights of 10–15 mg and reductant flow rates of 12 ml/min were used for all the experiments. A temperature ramp of 3, 7 and 21 °C/min from room temperature to 900 °C was used for all temperature-programmed reduction experiments.

3. Results

3.1. Theory

Consider a reaction:

gas + solid → product

The reaction can be described by an equation:

$$\text{rate} = \frac{-[\text{gas}]}{\mathrm{d}t} = k(T)[\text{gas}]^n \quad (1)$$

where [gas] is gas concentration, n the order of reaction and, k the rate constant given by the Arrhenius equation, where T the Kelvin temperature, R the gas constant and E is the activation energy.

$$k(T) = A\,\mathrm{e}^{-E/RT} \quad (2)$$

Let α be the fraction reacted of solid reactant, and n be the reaction order. A simplified mathematical form of the reaction kinetics can be described as

$$f(\alpha) = (1-\alpha)^n$$

And the reaction rate can be written as

$$\frac{\mathrm{d}\alpha}{\mathrm{d}t} = k(T)\,f(\alpha) \quad (3)$$

Integration (3), yields

$$\int_0^\alpha \frac{\mathrm{d}\alpha}{f(\alpha)} = g(\alpha) = k(T)t$$

In TPR process, temperature is also a function of time, thus:

$$\psi = \frac{\mathrm{d}T}{\mathrm{d}t} \quad (4)$$

where ψ is the constant heating rate in the TPR experiment.

Thus, $g(\alpha)$ indicates the function related only on fraction conversion α, and the temperature T. The concepts are found suitable for obtaining kinetic processes under different conditions. However, this form of $f(\alpha)$ can not describe kinetics of nucleation or diffusion process. Four types of $f(\alpha)$ [5,14] are given in Table 1 which are some gas–solid reaction models based on kinetic studies: the Avarmi–Erofeev model is concerned with the nucleation process from the statistical probability treatment [15,16]; the unimolecular model is expected to be a first order reaction,

Table 1
The $f(\alpha)$ and $g(\alpha)$ function of different reduction models

Reduction model	$f(\alpha)$	$g(\alpha)$[c]
Three-dimensional nucleation according to Avarmi–Erofeev	$(1-\alpha)(-\ln(1-\alpha))^{2/3}$	$(-3\ln(1-\alpha))^{1/3}$
Two-dimensional nucleation according to Avarmi–Erofeev	$(1-\alpha)(-2\ln(1-\alpha))^{1/2}$	$(-2\ln(1-\alpha))^{1/2}$
Unimolecular decay	$1-\alpha$	$-\ln(1-\alpha)$
Three-dimensional diffusion according to Jander[a,b]	$3/2(1-\alpha)^{1/3}((1-\alpha)^{-1/3}-1)^{-1}$	$(1-(1-\alpha)^{1/3})^2$

[a] This model is geometrically defined as shrinking/unreacted core or contraction sphere models, with reaction proceeding topochemically.
[b] Gas diffusion through the product layer as the rate-determining step.
[c] $g(\alpha)=\int_0^\alpha \frac{d\alpha}{f(\alpha)}$.

and the three-dimensional diffusion model [17] is according to the Jander equation which assuming the reaction is proceeding equally in all faces of the particles, and the reaction rate is diminishing as a consequence of increasing thickness of the barrier layer.

Combination of Eqs. (2)–(4) leads to:

$$\frac{d\alpha}{dT}=\frac{1}{\psi}k(T)f(\alpha)=\frac{A}{\psi}e^{-E/RT}f(\alpha) \tag{5}$$

where

$$k(T)=Ae^{-E/RT}$$

Thus TPR patterns $d\alpha/dT$ versus T can be calculated by integrating Eq. (5):

$$\int_0^\alpha \frac{d\alpha}{f(\alpha)}=\frac{A}{\psi}\int_{T_0}^{T}e^{-E/RT}dT=g(\alpha)$$

Combining (4), (5), the integration can be solved by partial integration method [18,19]:

$$g(\alpha)=\frac{AE}{R\psi}P(x) \tag{6}$$

where

$$x=\frac{E}{RT}$$

Doyle [19] has tabulated the most commonly found values of $P(x)$:

$$P(x)=\int_x^\infty \frac{e^{-u}}{u^2}=\frac{e^{-x}}{x}-Ei(-x)$$

$$Ei(-x)=-\int_x^\infty e^{-u}$$

And for computing purposes, $P(x)$ can be approaches by the following simplification:

$$P(x)=\frac{e^{-x}}{x}\left(\frac{674.567+57.421x-6.055x^2-x^3}{1699.066+841.655x+49.313x^2-8.02x^3-x^4}\right)$$

The integration approaching equation can be used for $9\le x\le 174$ [18]. Thus functions of $g(\alpha(T))$ and $f(\alpha(T))$ are given, and combine Eqs. (5) and (6) one can get the simulation TPR pattern:

$$\frac{d\alpha}{dT}=\frac{A}{\psi}e^{-E/RT}f(\alpha)=\frac{A}{\psi}e^{-E/RT}f(\alpha(T)$$

where A and E were calculated by experimental data.

Since the maximum reaction rate occurs TPR peak,

$$\left[\frac{d}{dT}\left(\frac{d\alpha}{dT}\right)\right]_{T=T_{max}}=0$$

Then,

$$\frac{d}{dT}\left[\frac{A}{\psi}e^{-E/RT}f(\alpha)\right]_{T=T_{max}}=\frac{E}{RT_{max}^2}\frac{A}{\psi}e^{-E/RT_{max}}f(\alpha)+\frac{A}{\psi}e^{-E/RT_{max}}\times\left(\frac{df(\alpha)}{d\alpha}\right)_{T=T_{max}}\left(\frac{d\alpha}{dT}\right)_{T_{max}}=0$$

From Eq. (5), $f(\alpha)=(d\alpha/dT)(\psi/A)(e^{E/RT})$Thus the equation becomes:

$$\left(\frac{d\alpha}{dT}\right)_{T=T_{max}}\times\left[\frac{E}{RT_{max}^2}+\frac{A}{\psi}e^{-E/RT_{max}}\left(\frac{df(\alpha)}{d\alpha}\right)_{T=T_{max}}\right]=0 \tag{7}$$

Since $(d\alpha/dT)_{T=T_{max}} \neq 0$, Eq. (7) can be reduced to

$$\left[\frac{E}{RT_{max}^2} + \frac{A}{\psi} e^{-E/RT_{max}} \left(\frac{df(\alpha)}{d\alpha}\right)_{T=T_{max}}\right] = 0 \quad (8)$$

Thus A can be calculated by:

$$A = \frac{-E}{RT_{max}^2} \times \frac{\psi e^{E/RT_{max}}}{(df(\alpha)/d\alpha)_{T=T_{max}}} \quad (9)$$

From Eq. (8) one has:

$$\ln\left(\frac{\psi}{T_{max}^2}\right) = \frac{-E}{RT_{max}} - \ln\left(\frac{E}{AR}\right) + C \quad (10)$$

where $(df(\alpha)/d\alpha)_{T=T_{max}}$ is assumed as a constant C since reduction mechanism at the TPR peak did not change with heating rate.

Plotting $\ln(\psi/T_{max}^2)$ versus T_{max}^2 leads to a temperature-programmed Arrhenius plot, in which the slope is equal to $-E/R$.

3.2. Results

TPR of iron catalysts were carried out using H_2/N_2 mixtures with a flow rate of 60 ml/min. Fig. 1 contains a series of TPR profiles for precalcined iron samples, obtained at temperature ramping rates of 3, 7, and 21 °C/min. The typical hydrogen reduction profiles present the two-stage reductions which have been reported by other workers [20–22]. An increase in heating rate from 3 to 20 °C produced increases in T, of

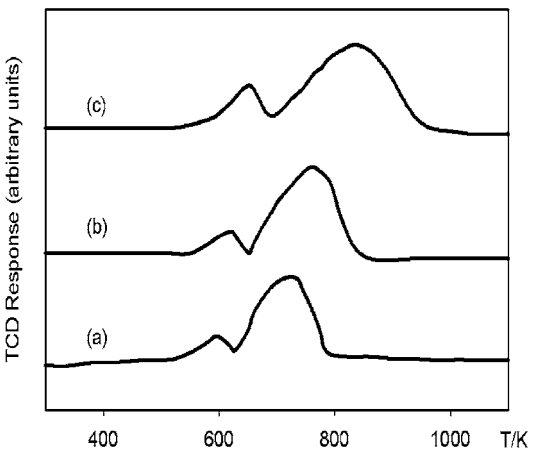

Fig. 1. TPR patterns of different heating rates (a) $\psi = 3\,(\mathrm{K\,min^{-1}})$; (b) $\psi = 7\,(\mathrm{K\,min^{-1}})$; (c) $\psi = 21\,(\mathrm{K\,min^{-1}})$.

~50 and ~100 °C for the first and the second step of iron reduction, respectively. The peaks at about 570 K in all profiles of Fig. 1 are due to the reduction of Fe_2O_3 to Fe_3O_4:

$$3Fe_2O_3 + H_2 \rightarrow 2Fe_3O_4 + H_2O \quad (11)$$

The peaks whose maxima were located about 770 K were due to the second reduction step from Fe_3O_4 to the metallic iron:

$$Fe_3O_4 + 4H_2 \rightarrow 3Fe + 4H_2O \quad (12)$$

According to Eq. (12), the ratio of the first peak area to second in the TPR profiles should be 1:8, provide that the reduction has been completed. Computing the peak area in Fig. 1, an average value of 11% of hydrogen was consumed in the first reduction step, in good agreement with the theoretical prediction. However, the peak area of the second reduction step is only 66%, lower than the theoretical value of 89%. This indicates that the second reduction step is incomplete.

Fig. 2 is the Arrhenius plot of the reaction which is plotted by Eq. (10), and the activation energies of both reduction steps can be calculated form the slop. The E values of 89.13 and 70.412 ($\mathrm{kJ\,mol^{-1}}$) were determined for the two steps, respectively.

Using Eq. (9), activation energy, T_{max} and $f(\alpha)$ of the four-reduction models from Table 1, the A values of the two-reductions step could be calculated. With the A values, the TPR pattern of different reduction models could be calculated by using Eq. (5). Table 2 shows the calculated A values of the two reduction steps and Fig. 3 shows the calculated TPR pattern. Compare the figure with the experiment TPR pattern, it is concluded that the calculated TPR pattern of unimolecular model fits best for the first reduction step: $Fe_2O_3 \rightarrow Fe_3O_4$, and the two-dimensional nucleation model according to Avrami–Erofeev describes the second reduction step: $Fe_3O_4 \rightarrow Fe$ best.

Fig. 4 shows TPR patterns of different heating rate (a) $\psi = 3\,(\mathrm{K\,min^{-1}})$; (b) $\psi = 7\,(\mathrm{K\,min^{-1}})$; (c) $\psi = 21\,(\mathrm{K\,min^{-1}})$ compared with calculated data. The solid lines are experimental data and dash-dot-dot lines are the calculated data by unimolecular for peak 1 and two-dimensional nucleation according to Avarmi–Erofeev model for peak 2. It is shown that the calculation patterns fit quite well with the TPR profiles for all three experiments of different heating rate.

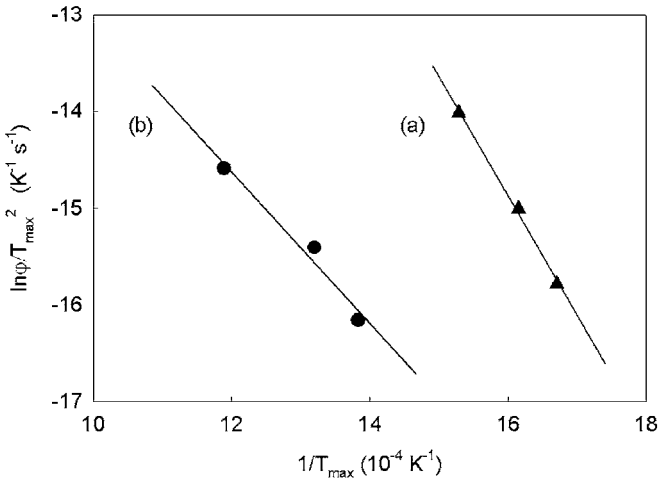

Fig. 2. Temperature-programmed Arrhenius plots for the two-step reduction. (a) $Fe_2O_3 \rightarrow Fe_3O_4$, (b) $Fe_3O_4 \rightarrow Fe$.

Table 2
A values of the two-reaction steps calculated by using $E = 89.13\,(\mathrm{kJ\,mol^{-1}})$, $T_{max} = 598.5\,\mathrm{K}$ for the first reduction step $Fe_2O_3 \rightarrow Fe_3O_4$, $E = 70.41\,(\mathrm{kJ\,mol^{-1}})$, $T_{max} = 723.2\,\mathrm{K}$ for the second reduction step $Fe_3O_4 \rightarrow Fe$, and $\psi = 7\,\mathrm{K\,min^{-1}}$

Reduction model	A, s^{-1} for $Fe_2O_3 \rightarrow Fe_3O_4$	A, s^{-1} for $Fe_3O_4 \rightarrow Fe$
Three-dimensional nucleation according to Avarmi–Erofeev	166.3700	1.46×10^5
Two-dimensional nucleation according to Avarmi–Erofeev	105.3500	9.22×10^4
Unimolecular decay	122.7900	1.07×10^5
Three-dimensional diffusion according to Jander	16.6800	1.46×10^4

3.3. Discussion

The TPR simulation patterns methods can be applied to determine the mechanism of the reduction reaction. Wimmers et al [5] have calculated the TPR pattern of the second peak for $Fe_3O_4 \rightarrow Fe$ step, but the first reduction peak was too low of an accurate quantitative analysis due to the sample size, so the $Fe_2O_3 \rightarrow Fe_3O_4$ step was not studied. In this work we observed the first peak of $Fe_2O_3 \rightarrow Fe_3O_4$ with a shoulder appearing on the low temperature side, and the good fit of the unimolecular model indicates that the first reduction step is a first order reaction: $r = Ae^{-E/RT}(1-\alpha)$ where A and E are listed in Table 3.

The second peak of the $Fe_3O_4 \rightarrow Fe$ was fitted with the two-dimensional nucleation model of Avrami–Erofeev. The general form of Avrami–Erofeev equation is:

$$[-\ln(1-\alpha)]^{1/n} = k(t - t_0)$$

Table 3
A values of the two-reaction steps calculated by using $E = 89.13\,(\mathrm{kJ\,mol^{-1}})$, $T_{max} = 598.5\,\mathrm{K}$ for the first reduction step $Fe_2O_3 \rightarrow Fe_3O_4$, $E = 70.41\,(\mathrm{kJ\,mol^{-1}})$, $T_{max} = 723.2\,\mathrm{K}$ for the second reduction step $Fe_3O_4 \rightarrow Fe$

Reduction model ($\mathrm{K\,min^{-1}}$)	A, s^{-1} for $Fe_2O_3 \rightarrow Fe_3O_4$	A, s^{-1} for $Fe_3O_4 \rightarrow Fe$
$\psi = 3$	98.62	9×10^4
$\psi = 7$	122.7900	1.07×10^5
$\psi = 21$	99.14	1.16×10^5

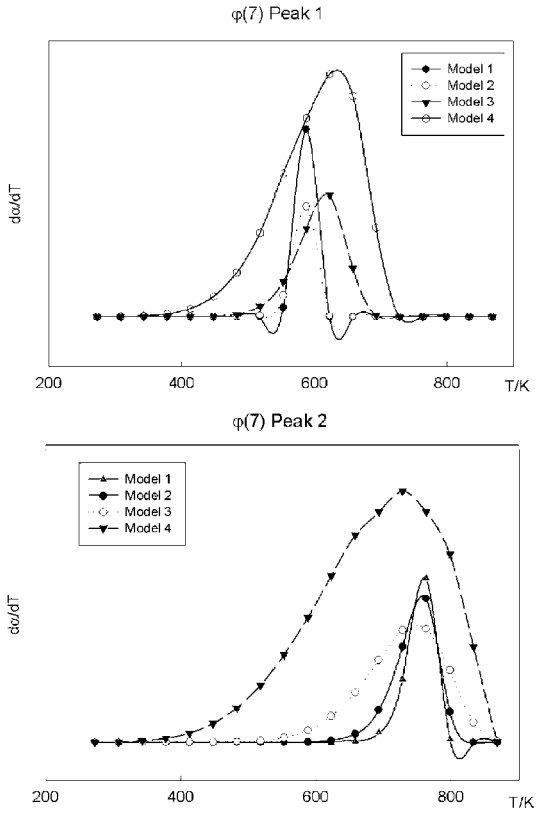

Fig. 3. Shows the TPR pattern of $\psi = 7\,(\mathrm{K\,min^{-1}})$ calculated by different reduction mode listed in Table 1.

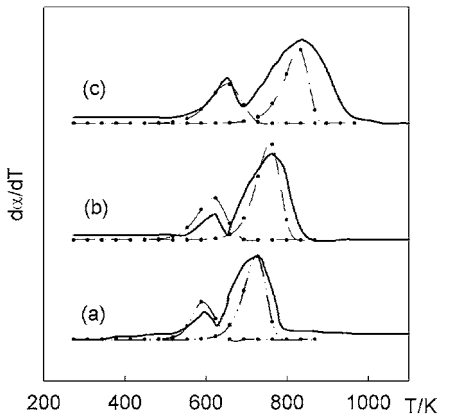

Fig. 4. TPR patterns of different heating rates compared with calculated data. The solid lines are measured data and dash–dot–dot lines are the calculated data by unimolecular for peak 1 and two-dimensional nucleation according to Avarmi–Erofeev model for peak 2. (a) $\psi = 3\,(\mathrm{K\,min^{-1}})$; (b) $\psi = 7\,(\mathrm{K\,min^{-1}})$; (c) $\psi = 21\,(\mathrm{K\,min^{-1}})$.

And the differential form of the Avrami–Erofeev equation is:

$$\frac{\mathrm{d}\alpha}{\mathrm{d}t} = nk^{1/n}[-\ln(1-\alpha)^{1-1/n}](1-\alpha)$$

The exponent $n = \beta + \lambda$ where β is the number of steps involved in nucleus formation (frequently $\beta = 1$ or 0, the latter corresponding to instantaneous nucleation) and λ is the number of dimensions in which the nuclei grow ($\lambda = 3$ for spheres or hemispheres, 2 for discs or cylinders and 1 for linear development). The equation can be used over a great of $\sim 0.05 < \alpha < 0.9$ for many solid phase reactions [14]. In this work the selection model is the two-dimensional nucleation model of Avrami–Erofeev, which is $n = 2$ for the general Avrami–Erofeev equation, where the in-situ formation of Fe_3O_4 indicated $\beta = 1$ and $\lambda = 2$, and the first-order nuclei formation of the interface is followed by linear growth of the nuclei in two dimensions.

4. Conclusion

Precipitated iron oxide samples were characterized using the temperature-programmed reduction method to investigate the reduction behaviors. The two-step reduction was observed. Fe_2O_3 was reduced to Fe_3O_4 and then reduce to metallic Fe. FeO was not detected as an intermediated. The activation energies for the two reduction steps of iron oxide were 89.13 and 70.41 ($\mathrm{kJ\,mol^{-1}}$). The simulation by reduction models of the TPR patterns presents well fitting of unimolecular model for $Fe_2O_3 \rightarrow Fe_3O_4$ reduction and two-dimensional nucleation according to Avarmi–Erofeev model for $Fe_3O_4 \rightarrow Fe$.

References

[1] J.W. Jenkins, B.D. McNicol, S.D. Robertson, Chem. Technol. 7 (1977) 316.
[2] C. Li, Y.W. Chen, Thermochim. Acta 256 (1995) 457.
[3] P. Arnoldy, J.C. M de Jonge, J.A. Moulijn, J. Phys. Chem. 89 (1985) 4517.
[4] N.W. Hurst, S.J. Gentry, A. Jones, B.D. McNicol, Catal. Rev. 24 (1982) 233.
[5] O.J. Wimmers, P. Arnoldy, J.A. Moulijn, J. Phys. Chem. 90 (1986) 1331.
[6] M. Sgunijawabe, R. Furuichi, T. Ishii, Thermochim. Acta 28 (1979) 287.

[7] A. Baranski, J.M. Langan, A. Pattek, A. Reizer, Appl. Catal. 3 (1982) 207.
[8] R. Brown, M.E. Copper, S.A. Whan, Appl. Catal. 3 (1982) 177.
[9] D.B. Bukur, X. Lang, J.A. Rossin, W.H. Zimmerman, M.P. Rosynek, E.B. Yeh, C. Li, Ind. Eng. Chem. Res. 28 (1989) 1130.
[10] D.B. Bukur, X. Lang, J.A. Rossin, W.H. Zimmerman, M.P. Rosynek, C. Li, Ind. Eng. Chem. Res. 29 (1990) 1588.
[11] H.E. Kissinger, Anal. Chem. 29 (1957) 1702.
[12] E.E. Unmuth, L.H. Schwartz, J.B. Butt, J. Catal. 63 (1980) 404.
[13] G. Munteanu, L. Ilieva, D. Andreeva, Thermochim. Acta 291 (1997) 171.
[14] L. G. Harrison, in:Comprehensive Chemical Kinetics, vol. 2, C. H. Bamford, C. F. H. Tipper (Eds.), Elsevier, Amsterdam, 1969, p. 57.
[15] M. Avrami, J. Chem. Phys. 7 (1939) 1103;
M. Avrami, J. Chem. Phys. 8 (1940) 212;
M. Avrami, J. Chem. Phys. 9 (1941) 117.
[16] B.V. Erofeev, C.R. Dokl. Acad. Sci URSS 52 (1946) 511.
[17] W. Jander, Z. Anorg. Allg. Chem. 163 (1927) 1;
W. Jander, Angew. Chem. 41 (1928) 79.
[18] J. Sesták, V. Satava, W.W. Wendtland, Thermochim. Acta 7 (1973) 333.
[19] C.D. Doyle, J. Appl. Polym. Sci. 5 (1961) 285.
[20] A. Lycourghiotis, D. Vattis, React. Kinet. Catal. Lett. 18 (1981) 377.
[21] A.J. Kock, H.M. Fortuin, J.W. Gecis, J. Catal. 96 (1985) 261.
[22] I.R. Leith, M.G. Howden, Appl. Catal. 37 (1988) 75.